Nigerian Journal of Theoretical and Environmental Physics (NJTEP)
ISSN Print: 3026-9601
ISSN Online: 1597-9849
DOI: https://doi.org/10.62292/njtep.v4i3.2026.172
Volume 4(3), September 2026

Short-Term Comparative Validation of IGS Final Global Ionospheric Map VTEC using Local GNSS Observations over Ogbomoso, Nigeria

***[1]Ogobor Efua Anthony, [1]Ayantunji Benjamin Gbenro, [1]Elemo Enoch Oluwaseun, [2]Adewumi Adebayo Segun, [1]Benjamin Joshua Olamide, [1]Mangete Otonyo, [1]Onuh Ochanya Blessing, and [1]Sani Abdulkadir Hauwa**

[1]Physical and Life Science Division, National Space Research and Development Agency, FCT Abuja, Nigeria.
[2]Department of Pure and Applied Physics, Ladoke Akintola University of Technology, Oyo State, Nigeria.

*Corresponding author's email: efuaogobor@gmail.com

ABSTRACT

Global Ionospheric Map (GIM) products are widely used for ionospheric research and Global Navigation Satellite System (GNSS) error assessment, but their ability to represent station-specific vertical Total Electron Content (VTEC) variations requires independent local validation. This study evaluates the agreement between station-derived VTEC and the International GNSS Service final GIM VTEC over Ogbomoso, Nigeria (8.1333°N, 4.2500°E). Local observations were obtained from an independently operated dual-frequency GNSS receiver whose data were not used in generating the evaluated GIM, thereby providing an external validation dataset. Corresponding IGS-GIM VTEC values, distributed in IONEX format, were spatially interpolated to the station coordinates and temporally interpolated from two-hourly to hourly resolution. A total of 1,005 matched hourly observations, comprising 333, 336, and 336 pairs from 14 selected observation days in May (1–16 May), June (3–17 June), and August (1–14 August) 2025, respectively, with some days excluded due to data unavailability, were analysed using diurnal and daily variations, scatter analysis, mean bias, mean absolute error, root mean square error, and Pearson correlation coefficient. Strong temporal agreement was obtained, with correlation coefficients of 0.969, 0.958, and 0.971 for May, June, and August, respectively. However, the IGS-GIM generally overestimated station-derived VTEC, with mean biases of 9.66, 6.15, and 3.23 TECU and corresponding RMSE values of 11.15, 7.96, and 5.37 TECU. The closest agreement occurred in August. Although the high correlations indicate strong temporal agreement, the observed biases and RMSE values reveal differences in absolute VTEC magnitude. The local GNSS-derived VTEC estimates are also subject to uncertainties associated with instrumental biases. These findings show that the IGS-GIM reproduced the broad temporal behaviour of VTEC during the selected periods but exhibited month-dependent magnitude differences, highlighting the need for independent local validation before its application to station-specific ionospheric and GNSS studies.

Keywords: GNSS, VTEC, GIM, Low-Latitude Ionosphere.

INTRODUCTION

The ionosphere is a region of the Earth's upper atmosphere extending approximately from 60 to 1000 km above the Earth's surface, where free electrons exist in sufficient concentrations to influence the propagation of electromagnetic radio waves. As a dispersive medium, the ionosphere introduces frequency-dependent group delay and phase advance into trans-ionospheric radio signals, including those transmitted by Global Navigation Satellite System (GNSS) satellites (Davies, 1990; Garner et al., 2008; Jakowski & Hoque, 2019). These ionospheric effects can be estimated using observations obtained at two GNSS frequencies. Consequently, dual-frequency GNSS receivers provide a reliable and cost-effective means of monitoring the thermosphere–ionosphere system through Total Electron Content (TEC) measurements (Cesaroni et al., 2020; Galkin et al., 2022). The low-latitude ionosphere is characterised by distinct electrodynamic processes, one of the most prominent being the Equatorial Ionization Anomaly (EIA) (Andima et al., 2019; Benjamin et al., 2025; Endeshaw & Radicella, 2026). The EIA is mainly

driven by the fountain effect, in which upward $E \times B$ plasma drift near the magnetic equator transports plasma to higher latitudes, forming two ionization crests on either side of the equator. In regions affected by the EIA, TEC varies significantly with latitude, longitude, altitude, season, and local time. Therefore, understanding the strength, location, and temporal evolution of the EIA crests is essential for interpreting TEC variability and improving GNSS-based applications in low-latitude regions (Olwendo et al., 2016; Cesaroni et al., 2020).

TEC represents the integrated number of free electrons along a specified propagation path (Andima et al., 2019; Cesaroni et al., 2020; Meng et al., 2024). TEC is expressed in Total Electron Content Units (TECU), where 1 TECU is equivalent to $1 \times 10^{16}\ electrons/m^2$. Slant TEC (STEC) refers to the electron content integrated along the satellite-to-receiver signal path, whereas vertical TEC (VTEC) represents the equivalent electron content within a vertical column through the ionosphere (Cooper et al., 2019; Ogobor et al., 2026). Variations in TEC affect GNSS signal propagation by producing ionospheric delay, phase advance, scintillation, Doppler shift, and refraction, thereby influencing positioning, navigation, and communication systems (Andima et al., 2019; Kenpankho et al., 2026). Since equatorial and low-latitude regions often experience high TEC variability, understanding and predicting TEC behaviour in these regions is important for accurate GNSS positioning and space-based applications (Meng et al., 2024). Several studies have investigated TEC variability over the African low-latitude region. For example, Olwendo et al. (2012), Habarulema et al. (2013), Andima et al. (2015), Amaechi et al. (2018, 2021), Idolor et al. (2022), and Endeshaw and Radicella (2026) examined diurnal, seasonal, quiet-time, and disturbed-time TEC characteristics across different parts of the African low-latitude ionosphere. These studies have contributed considerably to the understanding of ionospheric dynamics over Africa. Despite these contributions, independent station-level assessments of how accurately global ionospheric products reproduce local VTEC magnitude and temporal variability remain limited for several Nigerian low-latitude locations (Ikani et al., 2023).

Global Ionosphere Map (GIM) products generated by different International GNSS Service (IGS) ionosphere analysis centers can produce different TEC values and accuracy levels because they are based on different modelling strategies, station networks, and processing assumptions (Wielgosz et al., 2021; Li et al., 2023). Therefore, validation under different geographical, seasonal, solar activity, and ionospheric conditions is necessary before GIM VTEC is used as a substitute for local receiver-derived TEC (Hernández-Pajares et al., 2009). This is particularly important in low-latitude regions, where TEC variability is strong and can affect GNSS-based applications.

In Nigeria, GNSS-based studies have reported seasonal and diurnal VTEC variability, ionospheric irregularities, latitudinal differences, and TEC-related GNSS effects over low-latitude stations (Elemo et al., 2018; Ikani et al., 2023; Ogobor et al., 2026). In addition, previous studies have compared GPS/GNSS-derived TEC with empirical models and global ionospheric products. For example, Ogwala et al. (2022) investigated longitudinal TEC variations across the American, African, and Asian sectors during the descending and minimum phases of solar cycle 24 (2016–2019), comparing GPS-derived TEC with CODE-GIM and IRI-2016. Although their study included African GNSS stations in Cape Verde and Ethiopia, no observations from Nigerian GNSS stations were considered. Furthermore, their investigation primarily focused on longitudinal and seasonal TEC variability rather than the station-specific performance of the IGS final combined GIM over Nigeria. The IGS final combined GIM, unlike the individual CODE-GIM product, is generated from contributions of multiple IGS Ionospheric Associate Analysis Centres (Dach & Bockmann, 2025). Given the geographical variability of the low-latitude ionosphere and differences in global ionospheric products, these previous findings cannot necessarily establish the agreement between IGS final combined GIM VTEC and local GNSS-derived VTEC over Ogbomoso, Nigeria.

To address this gap, the present study uses independently acquired and processed local GNSS observations from the LAUTECH GNSS Laboratory (LGL), Ogbomoso, Nigeria, as a station-specific comparison dataset. Hourly TEC values obtained from the local GNSS receiver were compared with corresponding GIM VTEC values extracted at the same station coordinate. The analysis considered diurnal variation, daily mean TEC, correlation, bias, mean absolute error (MAE), and root mean square error (RMSE) to assess how well GIM VTEC represents local TEC variability and magnitude over the Nigerian low-latitude station. Correlation was used to assess temporal co-variation, while bias, MAE, and RMSE quantified differences in VTEC magnitude. The study also examined whether the agreement between the two datasets varied from month to month under different ionospheric conditions. The analysis is intended as a short-term station-level assessment and does not constitute a complete seasonal or solar-cycle validation. This study aims to evaluate the temporal agreement and magnitude differences between IGS final combined GIM VTEC and independently acquired and processed local GNSS-derived VTEC over Ogbomoso, Nigeria.

MATERIALS AND METHODS

This study was carried out over Ogbomoso, Oyo State, Nigeria, using TEC derived from two data sources: a

local GNSS receiver station and corresponding International GNSS Service (IGS) GIM VTEC extracted for the same geographic location. The local GNSS receiver is located at the LGL, Ogbomoso, at approximately 8.1333°N latitude, 4.2500°E longitude and 403.411 m ellipsoidal height. This station lies within the Nigerian low-latitude ionospheric region, where TEC variability is strongly influenced by equatorial ionospheric processes, including equatorial ionization anomaly effects, enhanced electron density gradients, and ionospheric irregularities that may affect GNSS signal propagation.

The location of the Ogbomoso GNSS receiver station is shown in Figure 1.

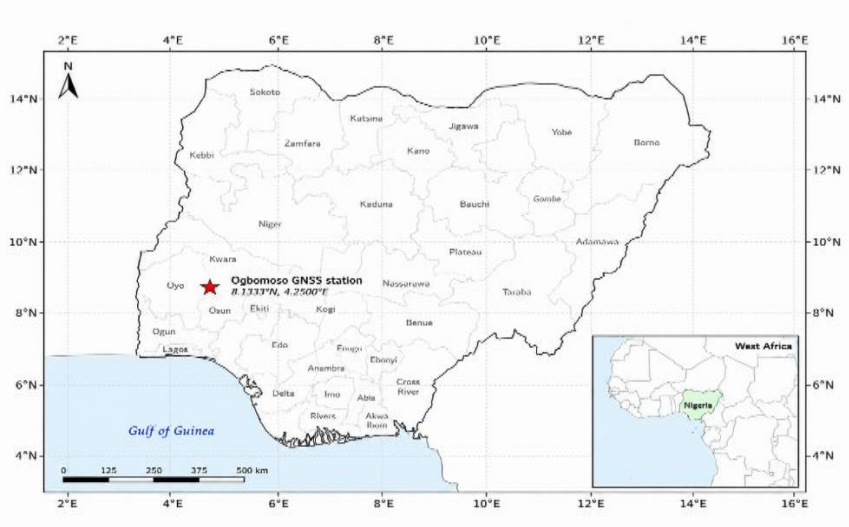


Figure 1: Location map of Nigeria showing the LGL receiver station

The local TEC data were obtained from GNSS observations recorded at LGL using a u-blox ZED-F9P dual-frequency GNSS receiver connected to a u-blox multiband GNSS patch antenna installed in an open-sky environment. The use of this receiver type is consistent with previous studies showing that compact dual-frequency u-blox receivers can provide useful GNSS observations for ionospheric monitoring and low-latitude GNSS applications (Dan et al., 2021; Adewumi et al., 2025; Ogobor et al., 2026). The receiver was operated in static observation mode, and raw GNSS observations were recorded at a sampling rate of 4 Hz. Only GPS observations were used for TEC estimation, specifically the L1 C/A (1575.42 MHz) and L2C (1227.60 MHz) signals, using the C1C–C2L pseudorange combination and corresponding L1C–L2L carrier-phase observations. A satellite elevation cutoff of 15° was applied to minimise low-elevation multipath effects. The raw data were initially logged in UBX format and then converted to Receiver Independent Exchange Format (RINEX 3.03) using RTKCONV in RTKLIB version 2.4.3 b34. The hourly RINEX files were subsequently merged into continuous daily observation files before TEC processing. The local GNSS observations were processed to obtain station-derived VTEC using GPS-GOPI version 3.05. Satellite differential code biases (DCBs) were obtained from the Center for Orbit Determination in Europe (CODE), while receiver DCBs were estimated during processing. The GPS-TEC processing procedure incorporates cycle-slip handling and carrier-phase levelling, whereby phase-derived TEC is levelled against code-derived TEC to reduce the influence of pseudorange noise and multipath. Continuous satellite observation arcs are treated separately when interrupted by data gaps (Seemala, 2023).

The TEC estimation from the local GNSS receiver is based on the dispersive nature of the ionosphere, where GNSS signals at different frequencies experience different propagation delays due to the presence of free electrons along the signal path. The VTEC represents the total number of electrons integrated along a vertical column through the ionosphere and is expressed as:

$$VTEC = \int_{h_{surface}}^{h_{ionosphere}} N_e dh \qquad (1)$$

Where N_e is the electron density, $h_{surface}$ represents the Earth's surface, and $h_{ionosphere}$ represents the upper boundary of the ionosphere. TEC is expressed in TEC units, where 1 TECU is equal to 10^{16} electrons per square metre (Dan et al., 2021; Ogobor et al., 2026). For a dual-frequency GNSS receiver, the code-derived slant TEC was obtained from the differential pseudorange measurements as:

$$STEC_p = \frac{f_2^2 \times f_1^2}{(f_2^2 - f_1^2) \times 40.3 \times 10^{16}} \times (P_1 - P_2) \quad (2)$$

where $STEC_p$ is the code-derived slant TEC expressed in TECU, P_1 and P_2 are the pseudorange measurements in metres, and f_1 and f_2 are the GPS L1 (1575.42 MHz) and L2 (1227.60 MHz) carrier frequencies, respectively. The frequencies are expressed in Hz when evaluating the equation, while the factor 10^{16} converts electron content from electrons/m² to TECU, where 1 TECU = 10^{16} electrons/m² (Dan et al., 2021).

The carrier-phase-derived slant TEC was expressed as:

$$STEC_\emptyset = \frac{f_2^2 \times f_1^2}{(f_1^2 - f_2^2) \times 40.3 \times 10^{16}} \times (\lambda_1 \emptyset_1 - \lambda_2 \emptyset_2) \quad (3)$$

Where $STEC_\emptyset$ represents the carrier-phase-derived slant TEC, λ_1 and λ_2 are the carrier wavelengths in metres, and $\emptyset_1$ and $\emptyset_2$ are the carrier-phase observations expressed in cycles. Unlike code-derived STEC, carrier-phase-derived STEC contains an unknown ambiguity offset and therefore provides relative TEC variations. Carrier-phase levelling against the code-derived STEC was applied to obtain absolute STEC estimates while reducing the influence of pseudorange noise and multipath (Dan et al., 2021; Seemala, 2023). Since measured slant TEC contains instrumental biases, satellite and receiver differential code biases were considered in obtaining the corrected slant TEC. The corrected slant TEC for the ith satellite was expressed as:

$$STEC_{true_i} = TEC_s + DCB_{sat_i} + DCB_{R_x} \quad (4)$$

Where TECs is the measured slant TEC for the ith GPS satellite, DCB_{sat_i} represents the satellite differential code bias correction, and DCBrx represents the receiver differential code bias correction, both expressed in TECU. The correction terms follow the additive convention adopted in Equation (4), whereby the satellite and receiver bias corrections are applied to the measured STEC to obtain the bias-corrected estimate. Satellite DCB products were obtained from CODE, while receiver DCBs were estimated using GPS-GOPI version 3.05. The corrected slant TEC was converted to vertical TEC using a single-layer mapping function. In this approach, the ionosphere was assumed to be concentrated in a thin shell at an ionospheric pierce point height of 350 km. The conversion was performed using the obliquity correction factor, $S(E)$, which accounts for the geometrical relationship between the slant propagation path and the corresponding vertical ionospheric column, as expressed in Equation (5). This factor is the reciprocal of the conventional slant mapping factor.

$$S(E) = \left[1 - \left(\frac{R_e \times cosE}{R_e + H}\right)^2\right]^{0.5} \quad (5)$$

Where S(E) is the obliquity correction factor, E is the satellite elevation angle, R_e is the mean radius of the Earth, and H is the assumed ionospheric shell height of 350 km (Dan et al., 2021).

The vertical TEC was then obtained as:

$$VTEC = STEC_{true} \times S(E) \quad (6)$$

Where $STEC_{true}$ is the bias-corrected slant TEC and S(E) is the obliquity correction factor defined in Equation (5). The corrected slant TEC is multiplied by S(E) to obtain the corresponding VTEC. Although the local GNSS observations provide an independent reference for evaluating the IGS-GIM product, the station-derived VTEC estimates are also subject to uncertainties associated with instrumental biases. To provide an independent comparison dataset for the same location, GIM VTEC was extracted at the Ogbomoso station coordinate (8.1333°N, 4.2500°E). The final IGS GIM products were accessed through the Crustal Dynamics Data Information System (CDDIS) archive of the National Aeronautics and Space Administration (NASA Crustal Dynamics Data Information System [CDDIS], 2025). The IGS final combined GIM products have a nominal spatial resolution of 2.5° in latitude and 5° in longitude, with a temporal resolution of 2 hours. The file names followed the IGS long-format naming convention, such as IGS0OPSFIN_YYYYDDD0000_01D_02H_GIM.INX, where YYYY represents the year and DDD represents the day of year.

For each IONEX file containing the IGS-GIM product, the latitude grid, longitude grid, exponent, temporal interval and number of TEC maps were read from the file header. The longitude convention was checked to ensure consistency with the GIM grid, particularly where the 0–360° longitude system was used. For each TEC map epoch, the gridded TEC values were read and scaled using the exponent provided in the IONEX header. Missing grid values identified by the IONEX code 9999 were treated as undefined (NaN). The TEC value at the Ogbomoso station was then obtained using bilinear spatial interpolation implemented with the MATLAB interp2 function, from the surrounding GIM grid points, as expressed in Equation (7). Spatial extrapolation beyond the IONEX grid boundaries was not permitted.

$$TEC_{IONEX} = interp2(Lon, Lat, TEC_{grid}, lon_0, lat_0) \quad (7)$$

Where TEC_{IONEX} is the GIM VTEC at the Ogbomoso station, Lon and Lat represent the longitude and latitude grids of the GIM map, TEC_{grid} is the gridded TEC map at a given epoch, and lon_0 and lat_0 are the longitude and latitude of the Ogbomoso GNSS receiver station. Since the GIM products were provided at 2-hour intervals, the extracted point TEC values were converted to hourly

values using first-order linear temporal interpolation implemented with the MATLAB interp1 function, as expressed in Equation (8). The original processing script removed the final 00:00 UTC map corresponding to the following day, where present. Consequently, the 23:00 UTC value was estimated using linear endpoint extrapolation when the last retained map epoch was 22:00 UTC. Missing intermediate hourly values were filled through linear interpolation where valid surrounding values were available. The resulting hourly GIM VTEC values were aligned with the local GNSS-derived VTEC observations by matching their corresponding dates and UTC hours. Only valid matched observations were retained for statistical comparison.

$$TEC_{hourly} = interp1(t_{IONEX}, TEC_{IONEX}, th) \quad (8)$$

where TEC_{hourly} is the interpolated hourly TEC value, t_{IONEX} represents the original GIM epoch times, TEC_{IONEX} represents the TEC values extracted from the GIM maps, and th represents the hourly time vector from 00:00 to 23:00 UTC. The comparison was carried out using 14 selected observation days in each of May, June, and August 2025, covering 1–16 May, 3–17 June, and 1–14 August, respectively. The selected days were not continuous in all months: observations for 10–11 May and 15 June were absent from the matched dataset. A total of 1,005 valid matched hourly observations were analysed, comprising 333 pairs in May, 336 pairs in June, and 336 pairs in August. In May, three hourly records (17:00–19:00 UTC on 9 May) were also absent from the matched dataset. These months were selected to assess the agreement between local GNSS receiver-derived TEC and GIM VTEC under different monthly ionospheric conditions. For each month, both datasets were arranged by date and UTC hour. To ensure a fair comparison, only observations with matching date and UTC hour in both datasets were retained. Each matched record therefore consisted of the date, UTC hour, IGS-GIM VTEC, and station-derived VTEC. The agreement between the GIM VTEC and the local GNSS receiver-derived TEC was evaluated using TEC difference, mean bias, mean absolute error, root mean square error, and Pearson correlation coefficient. The TEC difference at each matched epoch was calculated as:

$$\Delta TEC = TEC_{IONEX} - TEC_{Local} \quad (9)$$

Where ΔTEC is the difference between the two TEC estimates at the same date and UTC hour. The mean bias was calculated as:

$$Bias = \frac{\sum(\boldsymbol{TEC_{IONEX} - TEC_{Local}})}{N} \quad (10)$$

Where N is the total number of matched hourly observations. A positive bias indicates that GIM VTEC is higher than the local GNSS receiver-derived TEC, while a negative bias indicates that GIM VTEC is lower than the local station estimates.

The mean absolute error was calculated as:

$$MAE = \frac{\sum|\boldsymbol{TEC_{IONEX} - TEC_{Local}}|}{N} \quad (11)$$

Where MAE represents the average absolute difference between the GIM VTEC and the local GNSS receiver-derived TEC.

The root mean square error was calculated as:

$$RMSE = \sqrt{\frac{\sum[(TEC_{IONEX} - TEC_{Local})^2]}{N}} \quad (12)$$

Where RMSE represents the average magnitude of the difference between the GIM VTEC and the local GNSS receiver-derived TEC after squaring the individual differences and taking their square root. The Pearson correlation coefficient was used to assess the strength of the linear relationship between the two TEC datasets and was calculated as:

$$r = \frac{Cov(\boldsymbol{TEC_{IONEX}, TEC_{Local}})}{(\sigma_{IONEX} \times \sigma_{Local})} \quad (13)$$

where r is the correlation coefficient, $Cov(\boldsymbol{TEC_{IONEX}, TEC_{Local}})$ is the covariance between the GIM VTEC and the local GNSS receiver-derived TEC, σGIM is the standard deviation of the GIM-derived TEC, and σLocal is the standard deviation of the local GNSS receiver-derived TEC.

A sensitivity analysis was conducted to investigate the influence of spatial interpolation and temporal endpoint handling on the extracted IGS-GIM VTEC. Bilinear interpolation, adopted in the main study, was compared with nearest-neighbour interpolation using IGS final GIM products for all 14 selected observation days in May 2025 (1–9 and 12–16 May). Across 333 hourly GIM estimates, the mean absolute difference between the two methods was 0.469 TECU, with a root mean square difference of 0.569 TECU and a maximum absolute difference of 1.566 TECU. These results indicate that the choice of spatial interpolation produced relatively modest differences in the extracted GIM VTEC during the examined period. The sensitivity of temporal endpoint handling was also examined by comparing the original linear extrapolation procedure used to estimate GIM VTEC at 23:00 UTC with linear interpolation between the 22:00 UTC map and the following day's 00:00 UTC map. Across the 14 selected days, the mean absolute difference between the two approaches at 23:00 UTC was 2.353 TECU, with a root mean square difference of 2.991 TECU and a maximum absolute difference of 7.033 TECU. These findings demonstrate that the choice of temporal endpoint treatment can appreciably influence GIM VTEC estimates specifically at 23:00 UTC, rather than the entire hourly time series.

RESULTS AND DISCUSSION

Figure 2 shows the mean diurnal variation of GIM VTEC and local GNSS receiver-derived TEC over Ogbomoso for May, June, and August 2025. In all three months, both datasets followed the expected low-latitude diurnal TEC pattern, with low values during the early morning hours, a gradual increase after sunrise, enhanced daytime values, and a reduction during the night. This shows that the GIM product captured the general temporal behaviour of the local ionosphere over the study location. Previous studies have similarly shown that GIM products can reproduce large-scale TEC variability, although their accuracy varies with region, local time, season and ionospheric conditions (Hernández-Pajares et al., 2009; Wielgosz et al., 2021; Poniatowski et al., 2023; Adil et al., 2025).

In May, GIM VTEC ranged from 13.31 TECU at 04:00 UTC to 73.43 TECU at 14:00 UTC, while the local receiver-derived TEC ranged from 5.52 TECU at 04:00 UTC to 63.37 TECU at 14:00 UTC. Both datasets reached their peak at 14:00 UTC, indicating that the daytime TEC enhancement was captured by both sources. However, GIM VTEC was generally higher than the local TEC, with mean diurnal values of 44.32 TECU and 34.61 TECU, respectively, giving an average difference of about 9.71 TECU. Despite this general overestimation, the two curves were very close around 06:00 and 07:00 UTC, with a difference of only 0.40 TECU at 06:00 UTC and 1.30 TECU at 07:00 UTC.

In June, TEC values were generally lower than in May. GIM VTEC ranged from 8.36 TECU at 04:00 UTC to 54.82 TECU at 16:00 UTC, while the local TEC ranged from 5.49 TECU at 03:00 UTC to 47.59 TECU at 12:00 UTC. The mean diurnal TEC values were 33.65 TECU for GIM and 27.50 TECU for the local receiver, giving an average difference of about 6.15 TECU. Although GIM still mostly overestimated the local TEC, the difference was smaller than in May. A notable feature occurred at 06:00 UTC, where the local receiver-derived TEC was slightly higher than the GIM-derived TEC, giving a negative difference of about −1.74 TECU. At 07:00 UTC, both datasets became very close again, showing good agreement during the early post-sunrise period.

In August, the two datasets showed the closest agreement. GIM VTEC ranged from 9.26 TECU at 04:00 UTC to 58.16 TECU at 14:00 UTC, while the local TEC ranged from 5.47 TECU at 04:00 UTC to 55.03 TECU at 15:00 UTC. The mean diurnal values were 34.30 TECU for GIM and 31.07 TECU for the local receiver, giving the smallest average difference of about 3.23 TECU. The August curves were closely aligned for much of the day, especially during the morning increase and daytime peak period. The local TEC was also slightly higher than GIM at 06:00 and 07:00 UTC, with differences of −1.83 TECU and −1.61 TECU, respectively.

Figure 2 shows that GIM VTEC reproduced the timing and shape of the local TEC variation over Ogbomoso, but it generally overestimated TEC magnitude. The overestimation was strongest in May and weakest in August, confirming that the agreement between GIM VTEC and local GNSS receiver-derived TEC was month-dependent. The common diurnal pattern observed in both datasets is consistent with the dominant photochemical and electrodynamic processes controlling the low-latitude ionosphere. The low VTEC values during the early morning hours are associated with the absence of solar ionization and the continued loss of electrons through recombination during the night. Following sunrise, increasing solar extreme-ultraviolet radiation enhances ion production, resulting in the progressive increase in VTEC. At low latitudes, this daytime enhancement is further influenced by the equatorial fountain effect, through which the eastward electric field produces an upward E×B plasma drift near the magnetic equator.

The uplifted plasma subsequently diffuses along geomagnetic field lines and contributes to the development of the Equatorial Ionization Anomaly crests. The afternoon to evening reduction reflects the weakening of photoionization and the increasing influence of recombination after sunset. Similar diurnal VTEC behaviour has been reported over African equatorial and low-latitude stations by Olwendo et al. (2012), Andima et al. (2015), Elemo et al. (2018), and Cele et al. (2023).

The systematic tendency of the IGS-GIM to produce higher VTEC values than the local station may reflect differences in spatial representation and processing methodology between the two products. The IGS-GIM represents ionospheric conditions over a relatively coarse global grid and is generated using observations from a distributed network of GNSS stations and global modelling procedures. In contrast, the local GNSS receiver represents ionospheric conditions observed directly over the Ogbomoso station and its surrounding ionospheric pierce points. In a low-latitude region influenced by the Equatorial Ionization Anomaly, strong spatial gradients can occur over relatively short distances. Spatial interpolation from surrounding GIM grid points may therefore smooth or displace localized ionospheric structures and produce VTEC values that differ from those obtained at the station. Differences in differential code bias estimation, mapping-function assumptions,

receiver characteristics, and local observation geometry may also contribute to the observed magnitude differences.

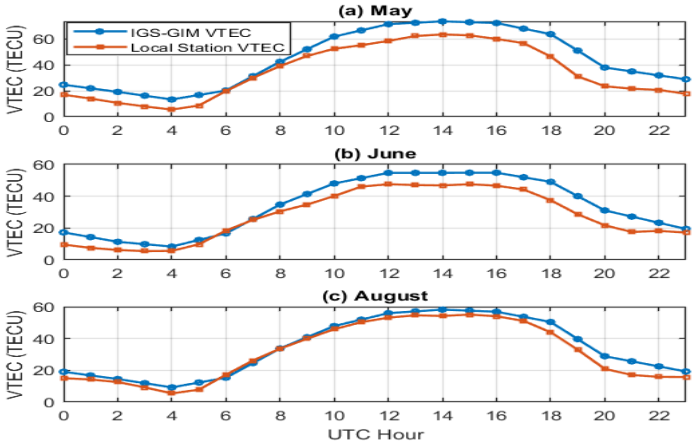


Figure 2: Mean diurnal variation of GIM VTEC and local GNSS receiver-derived TEC over Ogbomoso for selected two-week periods in May, June, and August 2025

Figure 3 shows the daily mean TEC comparison which provides further insight into how both datasets represented day-to-day TEC variability over the same location. Daily mean values were calculated from the matched hourly observations for each selected day, thereby allowing the consistency of GIM VTEC to be assessed beyond the hourly diurnal pattern. In May, GIM-derived daily mean TEC was consistently higher than local receiver-derived TEC. The GIM daily mean ranged from 37.06 TECU to 54.01 TECU, while local TEC ranged from 27.42 TECU to 41.76 TECU. The monthly average daily mean TEC was 44.14 TECU for GIM and 34.50 TECU for the local receiver, giving an average daily difference of 9.65 TECU. The largest daily difference was 14.71 TECU on 2 May, while the smallest was 5.77 TECU on 7 May. This shows that GIM captured the day-to-day variability but substantially overestimated the local station TEC during May.

In June, the daily mean TEC values were lower than those observed in May. GIM daily mean TEC ranged from 30.20 TECU to 36.96 TECU, while local TEC ranged from 22.78 TECU to 34.29 TECU. The average daily mean values were 33.65 TECU for GIM and 27.50 TECU for the local receiver, giving an average daily difference of 6.15 TECU. The highest daily difference was 9.57 TECU on 7 June. However, a negative daily difference of -3.61 TECU occurred on 14 June, indicating that the local TEC was higher than the GIM VTEC on that day. Despite this exception, GIM generally produced higher daily TEC values for most of the selected June days. In August, the daily mean comparison showed the closest agreement. GIM daily mean TEC ranged from 30.97 TECU to 39.46 TECU, while local TEC ranged from 25.23 TECU to 36.98 TECU. The average daily mean TEC was 34.30 TECU for GIM and 31.07 TECU for the local receiver, giving the smallest average daily difference of 3.23 TECU among the three months. The largest daily difference was 7.63 TECU on 14 August, while the smallest was -0.09 TECU on 8 August, showing that the two datasets were almost identical on that day.

The slight differences between the May mean diurnal difference (9.71 TECU), mean daily difference (9.65 TECU), and overall mean bias (9.66 TECU) arise from differences in averaging and the number of available observations. Of the 14 selected observation days, 13 contained 24 matched hourly observations, while 9 May contained only 21, with observations missing at 17:00–19:00 UTC. The mean diurnal difference was calculated by assigning equal weight to the 24-hourly means, whereas the mean daily difference assigned equal weight to the 14 daily means. In contrast, the overall mean bias was calculated directly from all 333 matched hourly observations. The small numerical differences therefore reflect the weighting of the available observations rather than inconsistencies in the TEC estimates.

Figure 3 further shows that the lowest daily mean TEC values across the entire observation period occurred on day 13 of June for both GIM VTEC and local GNSS

receiver-derived TEC. This simultaneous minimum suggests that both datasets captured the same reduction in ionospheric electron content on that observation day. However, an interesting feature was observed on 14 June 2025, when the local GNSS-derived VTEC exhibited a pronounced enhancement that was less evident in the IGS-GIM estimates. The local daily mean VTEC increased from 22.78 TECU on 13 June to 34.29 TECU on 14 June, representing an increase of approximately 11.51 TECU (50.5%). In contrast, the corresponding GIM VTEC increased only slightly from 30.20 to 30.68 TECU. The enhancement persisted over several consecutive hourly observations rather than occurring as an isolated measurement, with all 24 matched hourly records available for both days. Notably, this observation followed a period of enhanced geomagnetic activity, with planetary Kp reaching approximately 6 and Dst decreasing to about −101 nT on 13 June 2025 (National Oceanic and Atmospheric Administration [NOAA], 2025; NASA Goddard Space Flight Center, n.d.). The pronounced enhancement in local GNSS-derived VTEC on 14 June may therefore be associated with the preceding geomagnetic disturbance, which could have influenced ionospheric electron density and TEC variability over Ogbomoso. The comparatively weaker response in the IGS-GIM may reflect the limited spatial resolution of the global product, potentially smoothing short-term ionospheric variations.

The daily mean analysis confirms that GIM VTEC reproduced the broad day-to-day TEC behaviour over Ogbomoso but remained generally higher than local receiver-derived TEC. The average daily difference decreased from 9.65 TECU in May to 6.15 TECU in June and 3.23 TECU in August, indicating progressively closer agreement across the three selected observation periods. The month-to-month differences observed in Figure 3 further confirm that the agreement between GIM VTEC and local GNSS receiver-derived TEC was influenced by changing ionospheric conditions. The daily mean TEC values were relatively high in May, decreased in June during the solstice period, and increased again in August as the ionosphere gradually transitioned toward the September equinox season. This pattern shows that both datasets captured a part of the seasonal progression of TEC over Ogbomoso. This is consistent with previous studies over low-latitude regions, where TEC variability, ionospheric delay, and scintillation occurrence were shown to depend on season, local time, and solar-geophysical conditions (Cele et al., 2023; Ogobor et al., 2025; Ogobor et al., 2026). The reduction in daily mean VTEC from May to June, followed by an increase in August, may also be associated with changes in seasonal solar illumination, thermospheric composition, neutral winds, and low-latitude electrodynamics.

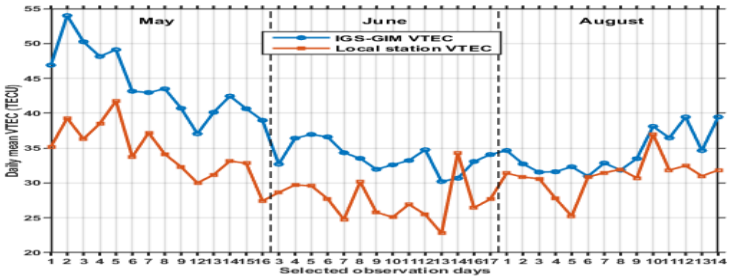


Figure 3: Daily mean GIM VTEC and local GNSS receiver-derived TEC over Ogbomoso for May, June, and August 2025

Figure 4 presents the scatter plots of matched hourly GIM VTEC against local GNSS receiver-derived TEC for May, June, and August 2025. The 1:1 reference line indicates perfect agreement, while the regression line shows the fitted relationship between both datasets. Points closer to the 1:1 line indicate better agreement in TEC magnitude, whereas wider displacement reflects differences between the GIM and local station estimates. The correlation coefficients show a strong positive relationship between the two datasets in all three months, with values of 0.969, 0.958, and 0.971 for May, June, and August, respectively. These values indicate that GIM VTEC closely followed the hourly variations of the local GNSS receiver-derived TEC, with the highest correlation observed in August. Further examination of the scatter plots revealed strong linear relationships between the two datasets. Using local GNSS-derived VTEC as the independent variable and GIM VTEC as the dependent variable, the fitted regression equations were GIM = 1.0352(Local) + 8.4420 for May, GIM = 1.0392(Local) + 5.0674 for June, and GIM = 0.9652(Local) + 4.3097 for August. The corresponding coefficients of determination

(R^2) were 0.9384, 0.9175, and 0.9438, respectively, indicating that the linear regression models explained approximately 93.84%, 91.75%, and 94.38% of the variation in GIM VTEC during the respective months. The regression slopes were close to unity, indicating comparable changes in GIM and local VTEC, while the positive intercepts and displacement of the scatter points from the 1:1 line revealed differences in their absolute magnitudes. These deviations were more pronounced in May and June, consistent with the larger positive biases reported earlier, whereas August showed comparatively better agreement. Although the correlation coefficients exceeded 0.95 across all three months, strong correlation primarily reflects the degree of co-variation between the datasets rather than equality in TEC magnitude. This explains why high correlations were obtained despite the appreciable mean biases and RMSE values, particularly in May. In general, the results demonstrate that the IGS-GIM reproduced the timing and broad temporal morphology of station-derived VTEC variations, although systematic differences remained in their absolute magnitudes.

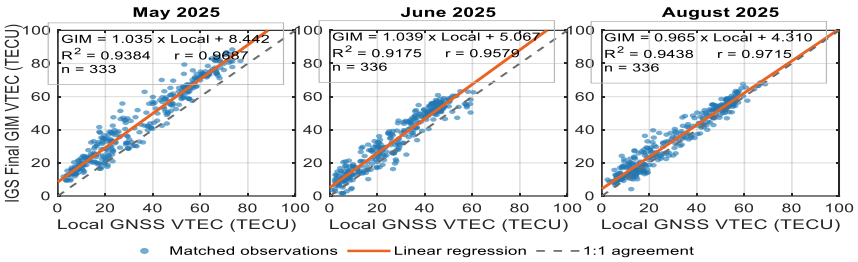


Figure 4: Scatter plots of IGS-GIM VTEC against local GNSS-derived VTEC over Ogbomoso for (a) May, (b) June, and (c) August 2025. Solid lines represent linear regression fits, while dashed lines indicate ideal 1:1 agreement

Among the selected observation periods, the agreement between IGS-GIM and local GNSS-derived VTEC was closest in August, followed by June and May, as indicated by the progressively smaller mean biases and RMSE values. However, this comparison is restricted to the sampled periods and should not be interpreted as evidence of a sustained seasonal trend.

Figure 5 presents the monthly error statistics used to quantify the agreement between GIM VTEC and local GNSS receiver-derived TEC over Ogbomoso. The statistical indicators considered were mean bias, mean absolute error (MAE), and root mean square error (RMSE). These metrics provide a direct measure of the difference between the GIM and local GNSS receiver-derived TEC values. The results show that May recorded the highest error values, with a bias of 9.66 TECU, MAE of 9.83 TECU, and RMSE of 11.15 TECU. This indicates that GIM VTEC overestimated the local station TEC most strongly in May. In June, the errors reduced to 6.15 TECU for bias, 6.90 TECU for MAE, and 7.96 TECU for RMSE, showing improved agreement compared with May. August recorded the lowest error values, with a bias of 3.23 TECU, MAE of 4.21 TECU, and RMSE of 5.37 TECU, confirming that it had the closest agreement between the two datasets. Generally, the reduction in bias from 9.66 TECU in May to 3.23 TECU in August, and the decrease in RMSE from 11.15 TECU to 5.37 TECU, show that the agreement between GIM VTEC and local GNSS receiver-derived TEC was month-dependent. The observed bias and RMSE are consistent with previous assessments showing that GIM accuracy is not spatially or temporally uniform and may deteriorate in equatorial and low-latitude regions where ionospheric gradients are strong (Hernández-Pajares et al., 2009; Wielgosz et al., 2021; Li et al., 2023; Poniatowski et al., 2023). The larger errors obtained in May may partly reflect the higher VTEC levels observed during that period, because errors associated with spatial interpolation, mapping functions, and model smoothing can increase when ionospheric electron density and horizontal gradients are enhanced. The progressive reduction in bias and RMSE from May to August may therefore indicate that the agreement depended partly on the prevailing VTEC magnitude and spatial structure rather than on a constant instrumental offset alone. Therefore, the lower error values in August and higher errors in May further emphasize the importance of locally validating GIM VTEC before applying it to station-specific ionospheric studies.

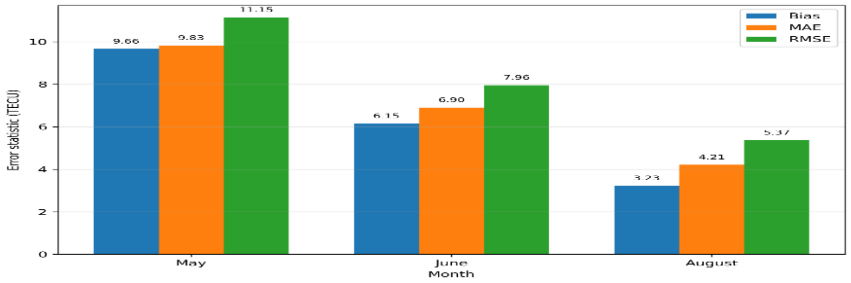


Figure 5: Monthly error statistics showing bias, MAE, and RMSE between GIM VTEC and local GNSS receiver-derived TEC over Ogbomoso for May, June, and August 2025

Figure 6 presents the mean hourly TEC difference between GIM VTEC and local GNSS receiver-derived TEC. The difference was calculated as GIM VTEC minus local GNSS receiver-derived TEC; therefore, positive values indicate GIM overestimation, while negative values indicate GIM underestimation. This analysis shows how the bias varied with UTC hour. In May, the hourly difference was mostly positive and reached its maximum value of 19.86 TECU at 19:00 UTC, showing the strongest GIM overestimation during the evening period. In June, the maximum difference reduced to 11.54 TECU at 18:00 UTC, while a slight underestimation occurred around 06:00 UTC. August showed the smallest hourly differences, with a maximum value of 8.58 TECU at 21:00 UTC and some early morning values close to or slightly below zero. The hourly difference analysis shows that the GIM bias was not constant throughout the day. Larger differences occurred mainly during daytime to evening hours, when TEC values were relatively high. This suggests that GIM overestimation became more pronounced during periods of TEC enhancement. The smaller differences in August further confirm that this month had the best agreement between GIM VTEC and local GNSS receiver-derived TEC. The local-time dependence of the VTEC difference may be related to the changing magnitude and spatial structure of the low-latitude ionosphere. During the early morning, electron density and horizontal gradients are generally weaker, which may partly explain the smaller differences between the datasets. During the daytime and evening, enhanced photoionization and equatorial electrodynamic processes increase VTEC and strengthen spatial gradients associated with the development of the Equatorial Ionization Anomaly. Under these conditions, a gridded global product may reproduce the broad temporal pattern without resolving the exact magnitude observed by a local receiver.

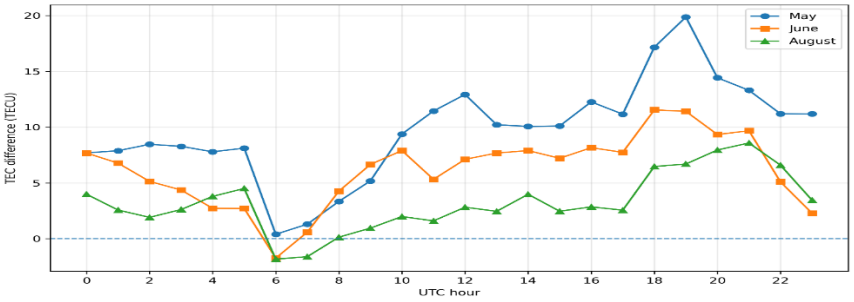


Figure 6: Mean hourly TEC difference between GIM VTEC and local GNSS receiver-derived TEC over Ogbomoso for May, June, and August 2025

Overall, the present results support earlier findings that global ionospheric maps reproduce broad and diurnal VTEC variability but may show systematic differences when evaluated at individual stations. Hernández-Pajares et al. (2009) demonstrated the usefulness of IGS VTEC maps for global ionospheric monitoring, while Wielgosz et al. (2021), Li et al. (2023), and Poniatowski et al. (2023) showed that GIM performance varies with region, product, solar activity, station distribution, and ionospheric conditions. The strong correlations obtained over Ogbomoso agree with the general ability of GIM products to capture broad temporal behaviour. However, the positive biases and larger May RMSE indicate that global consistency does not necessarily translate into

exact local agreement. This limitation is especially relevant over the African low-latitude sector, where GNSS station coverage is comparatively sparse and where the Equatorial Ionization Anomaly can produce strong spatial gradients that are difficult to resolve using global grids.

Conclusion

This study compared IGS-GIM VTEC with local GNSS receiver-derived TEC over Ogbomoso, Nigeria, using matched hourly observations from 14 selected days in each of May, June, and August 2025. The results showed that the GIM reproduced the general temporal behaviour of local TEC, including the early morning minimum, daytime increase, afternoon-to-evening enhancement, and nighttime reduction. Strong correlations were observed across the three sampled periods, indicating good agreement in temporal variations. However, the GIM generally overestimated local TEC, with the largest discrepancies observed in May and the smallest in August. These findings demonstrate that strong temporal agreement does not necessarily imply agreement in absolute TEC magnitude.

The findings are restricted to the selected observation days and should not be interpreted as evidence of seasonal or long-term GIM performance. Nevertheless, the IGS-GIM may serve as a complementary source for examining broad diurnal and day-to-day ionospheric variability over Ogbomoso. For applications requiring accurate station-specific TEC magnitudes, further local validation is necessary. Bias correction may be explored as a potential approach to reducing systematic differences, but its effectiveness would require development and evaluation using independent validation data. Future studies should extend the observation periods, examine different seasonal and geomagnetic conditions, and incorporate additional GNSS stations across Nigeria.

REFERENCES

Adewumi, A. S., Atilade, À. G., Abiodun, A. I., Ayantunji, G. B., Ogobor, E. A., Oyelowo, O., Fajobi, I., & Eleyele, D. E. (2025). PPP potential of a compact, low-cost GNSS receiver's module in a low latitude region: A case study at the LAUTECH GNSS Laboratory, Nigeria. In Proceedings of the 8th URSI-NG Annual Conference (URSI-NG 2024), *Advances in Physics Research (Vol. 12,* pp. 175–180). *Atlantis Press*. https://doi.org/10.2991/978-94-6463-644-4_17

Adil, M. A., Hadas, T., Yang, H., & Hernández-Pajares, M. (2025). Quality assessment of the real-time global ionospheric maps following varying solar dynamics and a severe geomagnetic storm. *GPS Solutions*, *29*, 58. https://doi.org/10.1007/s10291-024-01811-7

Amaechi, P. O., Oyeyemi, E. O., Akala, A. O., Kaab, M., Younas, W., Benkhaldoun, Z., Khan, M., & Mazaudier, C. A. (2021). Comparison of ionospheric anomalies over African equatorial/low-latitude region with IRI-2016 model predictions during the maximum phase of solar cycle 24. *Advances in Space Research, 68*(3), 1473–1484. https://doi.org/10.1016/j.asr.2021.03.040

Amaechi, P. O., Oyeyemi, E. O., & Akala, A. O. (2018). Geomagnetic storm effects on the occurrences of ionospheric irregularities over the African equatorial/low-latitude region. *Advances in Space Research, 61*(8), 2074–2090. https://doi.org/10.1016/j.asr.2018.01.035

Andima, G., Amabayo, E. B., Jurua, E., & Cilliers, P. J. (2019). Modeling of GPS total electron content over the African low-latitude region using empirical orthogonal functions. *Annales Geophysicae*, *37*(1), 65–76. https://doi.org/10.5194/angeo-37-65-2019

Andima, G., Jurua, E., Amabayo, E. B., & Habarulema, J. B. (2015). Statistical analysis of TEC perturbations over a low latitude region during 2009–2013 ascending solar activity phase. *Advances in Space Research*, *56*(11), 2542–2551. https://doi.org/10.1016/j.asr.2015.09.021

Benjamin, J. O., Okoh, D. I., & Rabiu, B. A. (2025). Global comparison of instantaneous electron density latitudinal profiles from Swarm satellites and IRI model. *Advances in Space Research*, *75*(8), 6454–6468. https://doi.org/10.1016/j.asr.2025.02.023

Cele, G., Andima, G., Habyarimana, V., & Jurua, E. (2023). Mapping of the ionospheric total electron content over the East African low-latitude region. *Advances in Space Research*, *71*(10), 4410–4423. https://doi.org/10.1016/j.asr.2023.01.006

Cesaroni, C., Spogli, L., Aragon-Angel, A., Fiocca, M., Dear, V., De Franceschi, G., & Romano, V. (2020). Neural network based model for global total electron content forecasting. *Journal of Space Weather and Space Climate*, *10*, Article 11. https://doi.org/10.1051/swsc/2020013

Cooper, C. M., Matsuo, T., Mannucci, A. J., Pi, X., Carter, B. A., & Shi, J. K. (2019). Measurement of

ionospheric total electron content using single-frequency geostationary satellite observations. *Radio Science*, *54*(1), 10–19. https://doi.org/10.1029/2018RS006575

Dach, R., & Bockmann, E. (Eds.). (2025). *International GNSS Service technical report 2024*. IGS Central Bureau and University of Bern. https://doi.org/10.48620/88697

Dan, S., Santra, A., Mahato, S., Koley, C., Banerjee, P., & Bose, A. (2021). On use of low-cost, compact GNSS receiver modules for ionosphere monitoring. *Radio Science*, *56*, e2021RS007344. https://doi.org/10.1029/2021RS007344

Davies, K. (1990). Ionospheric radio *(IEE Electromagnetic Waves Series, Vol. 31*). Peter Peregrinus Ltd., on behalf of the Institution of Electrical Engineers.

Endeshaw, L., & Radicella, S. M. (2026). Day-to-day longitudinal variability of total electron content (TEC) in the African equatorial region affected by the equatorial ionosphere anomaly. *Journal of Geophysical Research*: Space Physics, *131*(6), e2025JA035013. https://doi.org/10.1029/2025JA035013

Elemo, E. O., Ehigiator, M. O., & Ehigiator-Irughe, R. (2018). Seasonal variations of the Vertical Total Electron Content (VTEC) of the ionosphere at the GNSS COR station (SEERL) UNIBEN and three other CORS stations in Nigeria. *Nigerian Journal of Technology*, *37*(2), 286–293. https://doi.org/10.4314/njt.v37i2.1

Galkin, I., Froń, A., Reinisch, B., Hernández-Pajares, M., Krankowski, A., Nava, B., Bilitza, D., Kotulak, K., Flisek, P., Li, Z., Wang, N., Dollase, D. R., García-Rigo, A., & Batista, I. (2022). Global monitoring of ionospheric weather by GIRO and GNSS data fusion. *Atmosphere*, *13*(3), 371. https://doi.org/10.3390/atmos13030371

Garner, T. W., Gaussiran Ii, T. L., Tolman, B. W., Harris, R. B., Calfas, R. S., & Gallagher, H. (2008). Total electron content measurements in ionospheric physics. *Advances in Space Research, 42*(4), 720–726.

Habarulema, J. B., McKinnell, L. A., Burešová, D., Zhang, Y., Seemala, G., Ngwira, C., Chum, J., & Opperman, B. (2013). A comparative study of TEC response for the African equatorial and mid-latitudes during storm conditions. *Journal of Atmospheric and Solar-Terrestrial Physics*, *102*, 105–114. https://doi.org/10.1016/j.jastp.2013.05.008

Hernández-Pajares, M., Juan, J. M., Sanz, J., Orús, R., Garcia-Rigo, A., Feltens, J., Komjathy, A., Schaer, S. C., & Krankowski, A. (2009). The IGS VTEC maps: A reliable source of ionospheric information since 1998. *Journal of Geodesy*, *83*, 263–275. https://doi.org/10.1007/s00190-008-0266-1

Idolor, O. R., Akala, A. O., & Bolaji, O. S. (2022). African and American equatorial ionization anomaly (EIA) responses to 2013 SSW event. Journal of Geophysical Research: *Space Physics*, *127*(3), e2021JA029848. https://doi.org/10.1029/2021JA029848

Ikani, O. I., Okeke, F. N., Okpala, K. C., Okoh, D., & Rabiu, B. R. (2023). Diurnal and seasonal variations of the occurrence of ionospheric irregularities over Nigeria from GNSS data. *Frontiers in Astronomy and Space Sciences*, *10*, 1125950. https://doi.org/10.3389/fspas.2023.1125950

Jakowski, N., & Hoque, M. M. (2019). Estimation of spatial gradients and temporal variations of the total electron content using ground-based GNSS measurements. *Space Weather*, *17*(2), 339-356.

Kenpankho, P., Maichuen, S., Phothila, P., Zhang, J., Keokhumcheng, T., Ruttanaburee, S., & Pornsopin, P. (2026). GNSS Receiver Bias Model for Near Real Time TEC Monitoring at Low Latitude, Thailand. *Annals of Geophysics*, *69*(2), SA217-SA217.

Li, W., Wang, K., & Yuan, K. (2023). Performance and consistency of final global ionospheric maps from different IGS analysis centers. *Remote Sensing*, *15*(4), 1010. https://doi.org/10.3390/rs15041010

Meng, X., Verkhoglyadova, O. P., Chapman, S. C., Watkins, N. W., & Cafolla, M. (2024). Statistical characteristics of total electron content intensifications on global ionospheric maps. *Space Weather*, *22*(1), e2023SW003695.

NASA Crustal Dynamics Data Information System. (2025). *GNSS ionosphere and troposphere products*. NASA Earthdata. https://www.earthdata.nasa.gov/data/space-geodesy-techniques/gnss/atmospheric-products

NASA Goddard Space Flight Center. (n.d.). *Intense geomagnetic storm events* (2025, August 10). Coordinated Data Analysis Workshops. https://cdaw.gsfc.nasa.gov/CME_list/dst100/

National Oceanic and Atmospheric Administration. (2025, June 16). *Space weather highlights: 09 June–15 June 2025* (SWPC PRF 2598). *Space Weather Prediction Center*. https://www.ngdc.noaa.gov/stp/space-weather/swpc-products/weekly_reports/PRFs_of_SGD/2025/06/prf2598.pdf

Ogobor, E. A., Adewumi, A. S., Ayantunji, G. B., Haruna, M. S., Oyelowo, O., & Ogobor, E. A. (2026). Impact of ionospheric delay on GNSS in a low-latitude region: A case study of Ogbomoso, Nigeria. *Discover Electronics*, *3*, 32. https://doi.org/10.1007/s44291-026-00185-z

Ogobor, E. A., Adewumi, A. S., Ayantunji, G. B., Mohammed, S. H., Abiodun, A. I., Oyelowo, O., & Ogobor, E. A. (2025). Seasonal variability of ionospheric scintillation over LAUTECH, Ogbomoso, Nigeria. *International Journal of Maritime and Interdisciplinary Research*, *8*(1), 249–263.

Ogwala, A., Oyedokun, O. J., Ogunmodimu, O., Akala, A. O., Ali, M. A., Jamjareegulgarn, P., & Panda, S. K. (2022). Longitudinal variations in equatorial ionospheric TEC from GPS, global ionosphere map and international reference ionosphere-2016 during the descending and minimum phases of solar cycle 24. *Universe*, *8*(11), 575.

Olwendo, O. J., Yamazaki, Y., Cilliers, P. J., Baki, P., & Doherty, P. (2016). A study on the variability of ionospheric total electron content over the East African low-latitude region and storm time ionospheric variations. *Radio Science*, *51*(9), 1503-1518.

Olwendo, O. J., Baki, P., Mito, C., & Doherty, P. H. (2012). Characterization of ionospheric GPS total electron content (GPS–TEC) in low latitude zone over the Kenyan region during a very low solar activity phase. *Journal of Atmospheric and Solar-Terrestrial Physics*, 84–85, 52–61.

Poniatowski, M., Nykiel, G., Borries, C., & Szmytkowski, J. (2023). Spatio-temporal validation of GNSS-derived global ionosphere maps using 16 years of Jason satellites observations. *Remote Sensing*, *15*(20), 5053. https://doi.org/10.3390/rs15205053

Seemala, G. K. (2023). Estimation of ionospheric total electron content (TEC) from GNSS observations. In A. K. Singh & S. Tiwari (Eds.), *Atmospheric remote sensing: Principles and applications* (pp. 63–84). Elsevier. https://doi.org/10.1016/B978-0-323-99262-6.00022-5

Wielgosz, P., Milanowska, B., Krypiak-Gregorczyk, A., & Jarmołowski, W. (2021). Validation of GNSS-derived global ionosphere maps for different solar activity levels: Case studies for years 2014 and 2018. *GPS Solutions*, *25*, 103. https://doi.org/10.1007/s10291-021-01142-x